INTERNATIONAL JOURNAL FOR NUMERICAL METHODS IN FLUIDS, VOL. 15, 693–714 (1992)

OVERLAPPING GRIDS AND MULTIGRID METHODS FOR THREE-DIMENSIONAL UNSTEADY FLOW CALCULATIONS IN IC ENGINES

J. Y. TU AND L. FUCHS

Department of Gasdynamics, The Royal Institute of Technology, S-100 44, Stockholm, Sweden

SUMMARY

A new computational methodology with emphasis on using an overlapping grid technique and a multigrid method has been developed. The main feature of the present overlapping-grid system is of extended flexibility to deal with three-dimensional complex multicomponent geometries. The multigrid method is incorporated into this technique to accelerate the convergence of the numerical solution. The current scheme has been applied for computations of the laminar flows in the multicomponent configuration of internal combustion engines. The flow is governed by three-dimensional, time-dependent, incompressible Navier–Stokes equations with the continuity equation. A *time-independent* grid system is constructed for the moving boundary, i.e. the moving piston in the engine. This grid system is entirely different from others for the same problem in previous works. The performance of the present method has been validated by comparing the results with those from an equivalent, single-grid method and those from experiments. In addition, the flexibility and potential of the method has been demonstrated by calculating several cases which would be very difficult to be handled by other schemes.

KEY WORDS Overlapping grids Multigrid method Navier–Stokes equations Finite volume method Moving boundaries

1. INTRODUCTION

Most of the numerical methods for simulating flows in internal combustion (IC) engines are based on the approach that a single global time-dependent grid system is generated for the whole computational domain.[1] Numerical procedures for calculating flow fields are often based on the SIMPLE algorithm[2,3] or the vortex method.[4] Such an approach has led to the need for significant simplifications for the engine geometry. The computational domain has to be reduced to the extent that numerical grid generation techniques can handle and the boundary conditions have to be specified due to such a simplification. Most of the previous flow calculations have been performed for two-dimensional (2D) representation of IC engines either in planar[4] or in axisymmetrical forms.[5,6] Few three-dimensional (3D) calculations[7,8] have been carried out due to the long computational times being required to perform the calculations of engine flows on a computational grid which is fine enough to adequately resolve the spatial variations. Thus, a need exists for both numerical techniques that can readily treat more realistic engine configurations and numerical procedures that are robust and efficient. The work reported here is to develop a new computational methodology for IC engine flow calculations with emphasis on using overlapping-grid and multigrid (MG) methods.

0271–2091/92/180693–22$16.00

Received September 1991
Revised March 1992

A numerical grid generation technique involves mapping an irregular shape in the physical domain into a rectangular shape in the computational domain. Applications of this kind of technique to engine flow simulations have recently appeared in the literature.[9,10] Although grid generation techniques do help solve problems involving flow fields with arbitrarily shaped boundaries, it is obvious that as the configuration becomes more complex, the grid generation itself becomes a more difficult task. Construction of a single-grid system with appropriate resolution and mesh spacing that covers the entire flow field would be rather difficult for complicated flows such as the flow in an engine where both the intake (or exhaust) port flow and the in-cylinder flow are simultaneously considered.

An alternative way to remove these difficulties which has been employed in this study is to use an overlapping-grid technique by which a complex domain is divided into several geometrically simpler subdomains (or zones) which overlap each other. The grid in each zone is generated independently simply by using the existing grid generation schemes. The problem can be solved by computing alternatively a smaller problem in each zone and matching the local solutions by interpolation through the overlapping region. This approach has the potential to facilitate the use of different computational methods in different zones and also facilitate the use of parallel computational hardware. Moreover, the relative motion between the different parts of the computational domain can be accommodated by containing stationary parts in one (set of) zone(s) and moving parts in another (set of) zone(s).

This technique differs from some others which are often called patched-grid and multiblock techniques. Those techniques also use the idea of dividing the domain into a set of subdomains or blocks. However, these blocks are joined precisely together along some common boundaries (see e.g. References 11 and 12). The overlapping-grid technique is more flexible for the multicomponent configuration since the boundaries between the neighbouring zones do not need to strictly match or even be similarly aligned; consequently, completely differently orientated grid systems can be mixed for those complex multicomponent geometries. This method has been applied to the solution of the full-potential equations for transonic flows[13,14] and more recently applied to the computation of 2D incompressible[15] and compressible[16] flows. In this study, it has been applied to the calculations of the laminar flow governed by time-dependent, incompressible 3D Navier–Stokes equations in IC engine configurations.

In the IC engine problem, there is a moving piston which acts as the moving boundary. In most previous works,[3,5,7–10] a time-dependent grid that expands and compresses with the motion of the piston has been employed. This approach needs more computational time for regenerating new grids and redistributing computed results at each time step during the solution procedure. Moreover, the accumulation of errors due to the interpolation from the solution at the last time step to the new grids may impair the accuracy of the unsteady solution. In our case, however, a *time-independent grid system*, in which completely new grids are not necessarily generated at each time step, is constructed by using a local computational region attached to the moving piston. Such a concept is more important for the overlapping-grid system used with the MG solver since the two techniques can be naturally combined in this case.

The multigrid method is an iterative scheme developed originally for the solution of elliptic equations.[17] This scheme has been applied by Fuchs and Zhao[18] to the computation of 3D incompressible flows resulting in significant improvement in the convergence rate compared to the ordinary relaxation schemes. Here, this method has been incorporated into the present overlapping-grid technique to accelerate the convergence of solution. A correction scheme[14,19] in the interzonal information exchange is introduced to ensure global mass balance in each zone. This scheme makes the fast convergence of solution in the implementation of the multigrid technique possible in the overlapping-grid system.

A case for which the flow can be calculated equally well using an equivalent, single-grid method is chosen in this paper to validate and assess the performance of the multigrid method on overlapping grids. The flow in a model geometry of an engine with a central intake port is calculated to verify the computer code by comparison with existing experimental results. The numerical results for several cases which are very difficult when managed by other schemes are presented to demonstrate the flexibility and potential of the present scheme.

2. OVERLAPPING-GRID SYSTEM

The basic idea of the overlapping-grid technique used here is to employ a separate body-fitted grid for each component in a multicomponent configuration and then to interface the grids in a manner which allows an efficient solution of the governing equations. Two grid topologies for the configuration of the IC engine with off-centre intake and exhaust ports are illustrated in Figure 1. Three local body-fitted grids are generated for one straight-duct intake port, one exhaust port and the cylindrical combustion chamber, respectively, as shown in Figure 1(a). Two curved-duct ports are used in Figure 1(b) instead of the straight-duct ports of Figure 1(a). These local grids overlap where they meet, but are not required to collocate in the overlapping regions. When the domain may contain several solid bodies embedded in the computational domain, we flag the unused grid points in the zone so that the solid objects are excluded. On the edges of the unused points, the internal boundary points for the interfaces by interpolation between different zones are marked.[20] In this case, only those boundary points in one local grid which lie in others

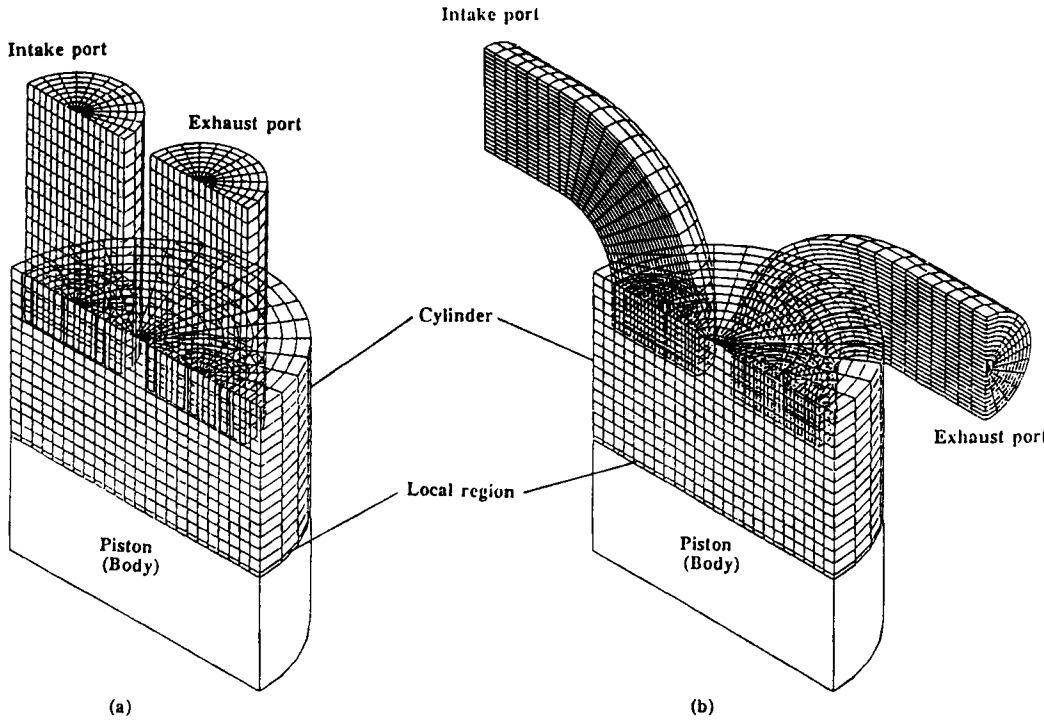

Figure 1. A 3D view of the overlapping-grid system for engine configurations

are marked for the interfaces and no unused grid point is needed to be flagged since there is no body within the computational domain. It should be noted, however, that in order to construct a time-independent grid system for the moving-boundary problem, the moving piston is treated artificially as a variable solid body in the computational domain. An overlapping-grid system is first generated for the piston lying at bottom dead centre (BDC), where the size of the body disappears. When the piston moves towards top dead centre (TDC) or from TDC to BDC, the size of the body will vary with the motion of piston and those grid points lying in the body will be flagged as unused points which are excluded from the calculation. Care should be taken when the piston face does not exactly lie on a grid plane. A local computational region, i.e. a thinner cell layer as illustrated in Figure 1, is allowed to attach to the piston. The main advantage of this time-independent grid system is that no mesh regeneration is required.

Compared to the single grid approach, the storage of numerical data for the overlapping grid system is more complicated. The data structure that we employ here is an extension of the multigrid data structure.[18,19] All the dependent variables and the grid parameters are stored in one-dimensional arrays. A pointer system is defined so that each subgrid can be accessed directly by an integer array $\mathrm{KGR}(m,n)$, where m is the grid level in the MG cycle and n is the subgrid index. The position of the first variable entry of each subgrid is calculated according to grid levels and the number of subgrids. The data is organized by grid levels as in the case of the multigrid scheme. Within each grid level, the variables of the first subgrid are stored at the beginning, followed by those of the second subgrid, and so on. The data for internal boundary points in different subgrids are also stored in additional shorter one-dimensional arrays and are independently managed by an auxiliary pointer system. Our numerical experience shows that this type of data structure allows access to each subgrid independently and it is easy to deal with the interfaces among the different grids. This grid system allows also addition/deletion of locally refined subgrids.[19]

3. GOVERNING EQUATIONS AND BOUNDARY CONDITIONS

3.1. Governing equations

The equations describing three-dimensional, time-dependent, incompressible, laminar flows in conservative, non-dimensional primitive variable formulation can be written as

continuity

$$\nabla \cdot \mathbf{U} = 0, \tag{1}$$

momentum

$$\frac{\partial \mathbf{U}}{\partial t} + \nabla \cdot (\mathbf{U}\mathbf{U}) = -\nabla P + \frac{1}{Re}\nabla^2 \mathbf{U}, \tag{2}$$

where $\mathbf{U} = (u, v, w)$ is the velocity vector, with Cartesian components in the x-, y- and z-direction, respectively; t indicates the dimensionless time; P represents the pressure; Re is the Reynolds number based on a reference velolcity, U_0, a reference length, D, and the kinematic viscosity, v.

3.2. Boundary conditions

There are potentially different types of boundaries, such as solid surfaces, inlets/outlets and 'internal surfaces'. No-slip condition is applied on solid surfaces and the velocity vector is assumed to be given at inlets/outlets. For the model engine problem, the velocity at the piston face is equal to the piston velocity and the inlet/outlet (uniformly distributed) velocity can be obtained

from the overall mass balance by

$$V_{io} = S_{piston}(\pi D^2/4)/A_e, \tag{3}$$

where S_{piston} is the piston speed, D the cylinder diameter and A_e the effective intake or exhaust area.

At 'internal' boundaries, the velocity vector is specified (the pressure is not required since no boundary condition is needed on the pressure for solving the governing equations and for the semi-stagged grids that we use). The velocity vector at the 'internal' boundary points is computed by interpolation during the iterative process. A three-dimensional Lagrange interpolation scheme is used and is implemented as a sequence of three one-dimensional interpolations. In this paper, a $4 \times 4 \times 4$ interpolation stencil is used to ensure the second-order accuracy of the numerical approximations to the solution of the governing equations.[16]

It should be noted that this kind of interpolation scheme does not guarantee the global mass conservation before convergence. It has been pointed out by Fuchs[15] that such an interface may prevent convergence and, in general, will slow down the convergence rate in the MG solver. Gu and Fuchs[14] introduced a mass conservative correction through the density for the solution of the full-potential equation. For the incompressible case it has been found that the addition of a correction to the interpolated values could improve the convergence rate without affecting the final solution.[19]

3.3. Initial conditions

For the model engine problem, the flow is time-dependent. At $t=0$, the piston is stationary at the TDC of the cylinder and the flow everywhere is set to be at rest. The flow inside the cylinder is driven by the motion of the piston away from the TDC, according to a simple harmonic motion, i.e. the motion of the piston follows a cosine wave while its velocity follows a sine wave. The position of the moving piston is given by

$$Z = L_c + \frac{L_s}{2}[1 - \cos(2b\pi t)], \tag{4}$$

where L_c is the clearance height of the cylinder and it is taken as $L_s/L_c = 5$; $2b\pi t$ refers to the crank angle θ, where b is the engine speed. Here the piston stroke is $L_s/D = 1{\cdot}0$ and the cylinder bore is $D = 1{\cdot}0$

4. NUMERICAL PROCEDURE

4.1. Discretization

The finite volume (FV) method is used to discretize the Navier–Stokes equations using Cartesian velocity components. By this approach one avoids the need for transformation of the co-ordinates and it makes the information exchange procedure among different grids simpler. We adopt a semi-staggered grid system in which all velocity components are defined at the cell vertex while the pressure (and, in fact, all scalar variables in the more complex flow simulations) is defined at the cell centre. The control volume for the continuity equation is the cell element itself. For the momentum equations, the control volume is formed by joining the cell centres surrounding the point of calculations. For details of the discretization by using FV approximations, see e.g. References 21 and 22. The FV approximation as implemented by us is given shortly in the following.

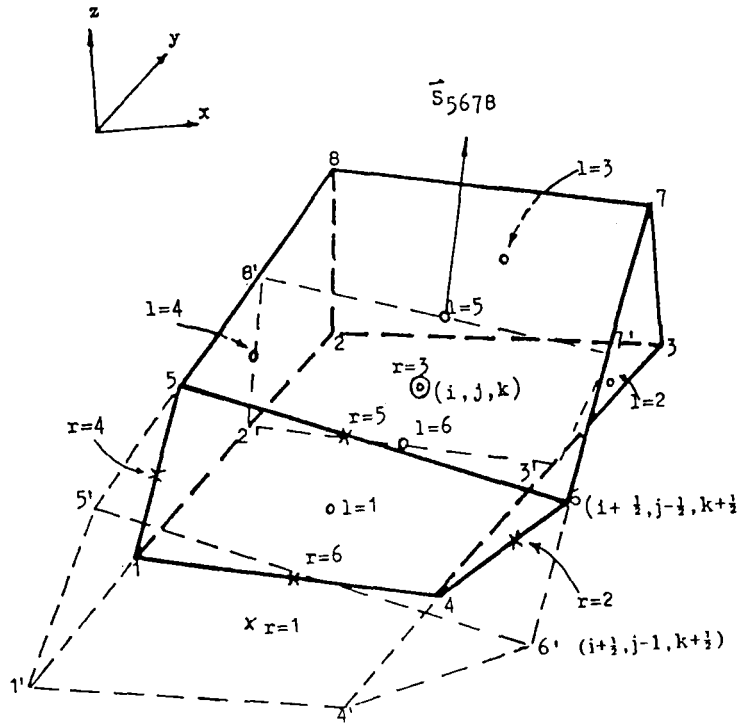

Figure 2. Illustration of main and subcontrol volumes in a physical space

We consider an arbitrary FV element for the momentum equations in the physical space as illustrated in Figure 2. A cell marked by the black solid lines indicates the main control volume which encloses a computational point in the cell centre. The dashed volume, called a subcontrol volume, encloses the central point of one surface of the main control volume. The following notations are used to discretize the first- and second-order derivatives. S_l^e indicates the projected area of the surface l of main control volume in the e-direction; S_{lr}^e indicates the projected area of the surface r of the subcontrol volume l in the e-direction; Φ_l and Φ_{lr} express the function values in the surface l of the main control volume and in the surface r of the subcontrol volume l, respectively; V and V_l are the volumes of the main and the subcontrol volume l, respectively; $l, r = 1, 2, \ldots, 6$; $e = 1, 2, 3, (x, y, z)$.

The first-order derivatives can be approximated as

$$\frac{\partial \Phi}{\partial x_e} = \lim_{V \to 0} \frac{1}{V} \int_V \frac{\partial \Phi}{\partial x_e} \mathrm{d}V = \lim_{V \to 0} \frac{1}{V} \int_S \Phi \, \mathrm{d}S^e \approx \frac{1}{V} \sum_{l=1}^{6} \Phi_l S_l^e \tag{5}$$

and the approximating Laplace's operator can be evaluated by

$$\nabla^2 \Phi = \lim_{V \to 0} \frac{1}{V} \int_S \nabla \Phi \cdot \mathrm{d}\mathbf{S} \approx \frac{1}{V} \sum_{e=1}^{3} \sum_{l=1}^{6} \frac{1}{V_l} \sum_{r=1}^{6} \Phi_{lr} S_{lr}^e S_l^e . \tag{6}$$

As seen, no co-ordinate and equation transformation is required and only the grid parameters such as areas and volumes of the cell have to be calculated in an efficient way.[23] It should be noted that a wedge-shaped control volume for the continuity equation and a control volume

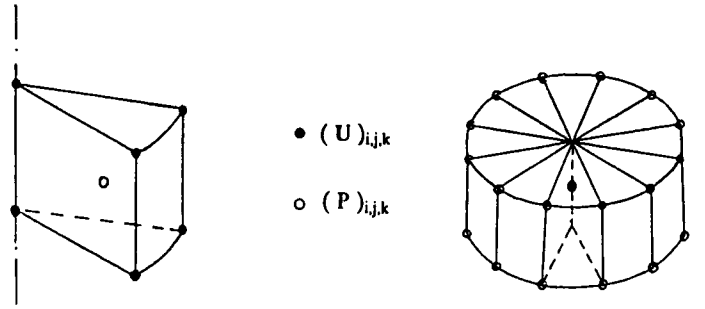

(a) for the continuity equation (b) for momentum equations

Figure 3. Illustrations of irregular control volume

which consists of multiple wedge-shaped volumes for momentum equations, as illustrated in Figure 3, are used for cases of degeneration (as near the axis of cylindrical co-ordinates).

The main advantage of using a semi-staggered grid system is that, on the one hand, it simplifies the treatment of cells of general shapes (collocation of velocity components). On the other hand, one does not have to specify boundary conditions on the pressure. The collocation of velocity components requires an additional 'dissipation' term into the continuity equation, to eliminate oscillation ('odd–even decoupling') in the pressure. This additional term is formally of fourth-order accuracy and, therefore, does not alter the total accuracy of the computed results.

The discretization formulation for the governing equations is implicit in time and the MG procedure is used to accelerate the convergence of the solution in each time step. The central difference approximation in equation (5) gives rise to high-frequency oscillations of the numerical solution in the case of high Reynolds number. The numerical damping used here is defined by a fourth-order difference operator which is similar to the scheme proposed by Jameson[24] for inviscid flows and applied to the viscous flow.[25]

4.2. Solution procedure

The multigrid procedure is used for the fast solution of discretized equations. More details of descriptions of MG methods for systems of equations and time-dependent problems (real-time-dependent or time-marching scheme towards steady state) can be found in References 18, 22, 26 and 27. Only those aspects that are directly relevant to the implementation on the overlapping-grid system will be described here.

The basic Schwarz algorithm implies that the discrete equations in each zone are solved before updating all the internal boundaries and the procedure is repeated until convergence is achieved. Previous numerical experiences[20,28] indicate that such an iterative process results in slow convergence and is sensitive to the extent of the overlap. Here, the updating procedure is an integral part of the MG cycle.

The solution procedure at each time step is as follows. A symmetrical line relaxation technique is used to smooth the three momentum equations. Then the continuity equation is relaxed pointwise, by updating all the dependent variables at each computational cell. The updating method is essentially close to the one described by Fuchs and Zhao.[18] Here, the correction for the velocity components and the pressure is carried out only at a single point (i.e. the one that is being relaxed). After minimal smoothing of the errors, the information is transferred among the grids by

interpolation at the points belonging to the internal boundaries. The interpolated values are corrected to ensure the total mass balance on each grid. The same relaxation procedure is performed successively in the other zones. Then the problems in all the zones are transferred to coarser grids using the FAS scheme[17] for the dependent variables and using the volume averaging restriction operator for the residuals. The corrections on the coarse grids are interpolated linearly to the fine grids. The iterations are carried out by a V-cycle MG process until a convergence solution is achieved.

In the model engine problem, the time steps are chosen so that the piston moves less than one mesh spacing on the finest grid in the piston-moving direction. This choice of the time step can be guaranteed independently of the spatial spacing since we use an implicit algorithm to march in time.

5. RESULTS

5.1. A 90° circular bend

A case for which the flow can be calculated by an equivalent, single-grid method is chosen to validate and assess the performance of the method developed above. The geometry consists of a 90° pipe bend with a mean radius of curvature of 3·2 times the diameter of the pipe, and inlet and outlet extensions of 2·0 and 3·2 times the diameter, respectively, (see Figure 4). The reason for choosing this case is that there is a large amount of experimental and numerical data for reference. Fully developed flow profile is given at the inlet and a zero-gradient condition is applied to the outlet. The Reynolds number, based on the maximum inlet velocity and the width at the inlet, is 150.

For reference purposes, the grid is artificially divided into three sections. On each of these, three grid levels are defined. The finest grids are $9 \times 26 \times 17$ for the inlet segment, $9 \times 26 \times 29$ for the bend and $9 \times 26 \times 21$ for the outlet segment. Figure 4 depicts the overlapping grids and some of the computed results. The secondary flows at 30°, 60° and at a distance of one diameter downstream from the end of the bend are shown in Figures 4(a)–4(c). Note that the scale factor of velocity vectors in Figures 4(a)–4(c) is 200 times larger than in Figure 4(d). From these figures it can be seen that the centre of the symmetrical pair of vortices caused by the centrifugal force moves from the inside to the outside of the pipe as the turning angle increases. It is also observed that the vortex motion weakens as it leaves the bend. In Figure 4(d), the velocity distribution in the mid-plane is presented. These results show a good agreement with the previously published numerical[29] and experimental[30] data.

In addition, a calculation is done using a single-grid system that is, in all other respects, equivalent to the method described in this report. The number of computational cells used in this calculation is $9 \times 26 \times 65$, which is close to the total number of all the three finest grids used in the overlapping-grid system. The MG procedure is also employed to this single-grid system by constructing a sequence of coarser grids. In this way, the performance of the overlapping grid scheme can be assessed by comparing single-grid calculations.

For the purpose of comparison, we freeze the pressure field and relax the momentum equations only. Figure 5 shows the convergence histories of the different calculations as function of work units (WU). One WU is the amount of work required to perform one sweep of symmetrical line relaxation on the finest grids. The work units required by the implementation of the interfaces on the overlapping-grid system are estimated by recording the required CPU time. It can be concluded that the current scheme is far more efficient than the single-grid scheme. The information exchange among the zones leads to some deteriorated convergence rate. The

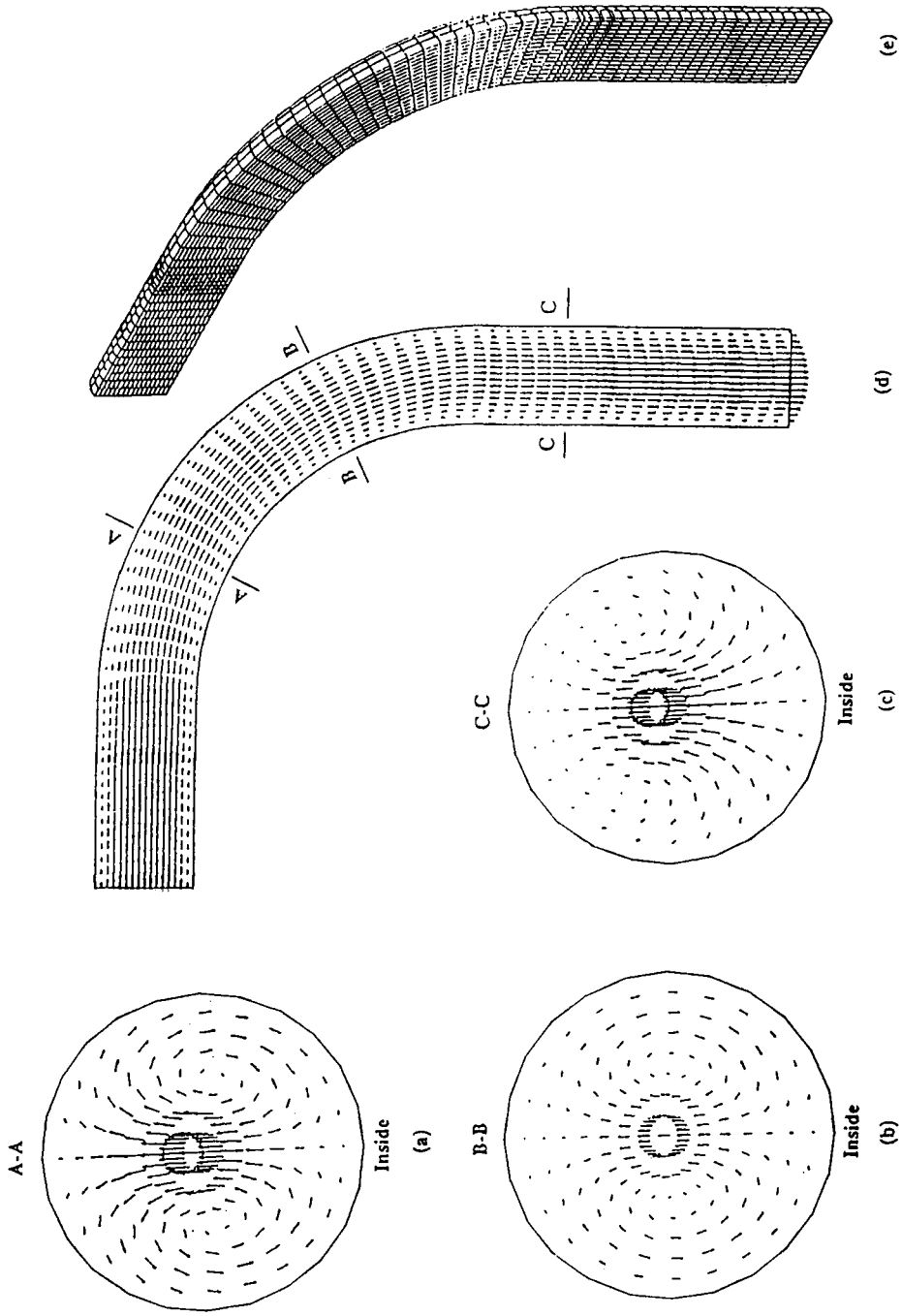

Figure 4. Velocity vector plots and 3D view of the overlapping-grid system

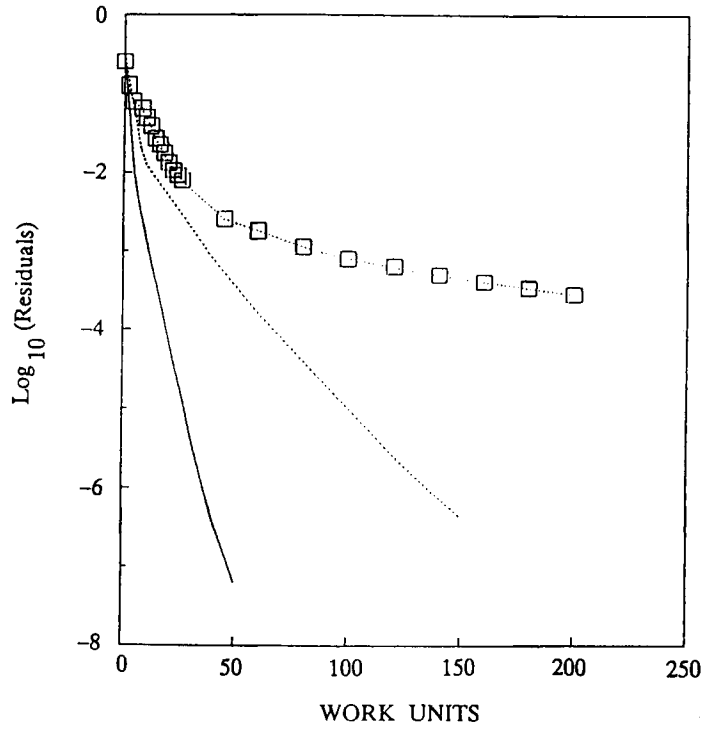

Figure 5. Convergence histories of the different schemes: ———, MG in the single-grid system; . . . . . MG in the overlapping-grid system; . . . □ . ., Single grid scheme in the single-grid system

overlapping-grid system is, however, far more flexible to deal with the complex geometry than a global single-grid system.

5.2. A chamber with a central intake port

The flow field in a model engine whose configuration has been used in the experimental investigation of Ekchian and Hoult[31] is calculated here. The experimental observations and published numerical computations are used for a comparison to verify the current computer code for the model engine problem. For all the engine problems studied in this paper, the Reynolds number based on the maximum piston velocity and the chamber diameter, is taken to be $Re = 150$. The overlapping-grid system for this case is similar to that of Figure 1(a), where the two ducts are replaced by a single duct aligned with the central line of the cylinder. The finest grids used are $13 \times 26 \times 17$ for the intake port and $13 \times 26 \times 29$ for the chamber, respectively. A fixed valve, 0·45 times the diameter of the cylinder, is located at the distance 0·12 times the stroke away from the head of the chamber. In the numerical calculation, it is assumed that the valve is fully opened during the entire intake process.

Figure 6(a) shows a three-dimensional velocity vector plot of the intake stroke flow at an equivalent crank angle (CA) of $\theta = 90°$. The interaction of the intake jet with the wall produces large-scale rotating flow patterns within the cylinder volume. The upper corner of the chamber contains a second smaller vortex rotating in the opposite direction. The flow around the valve

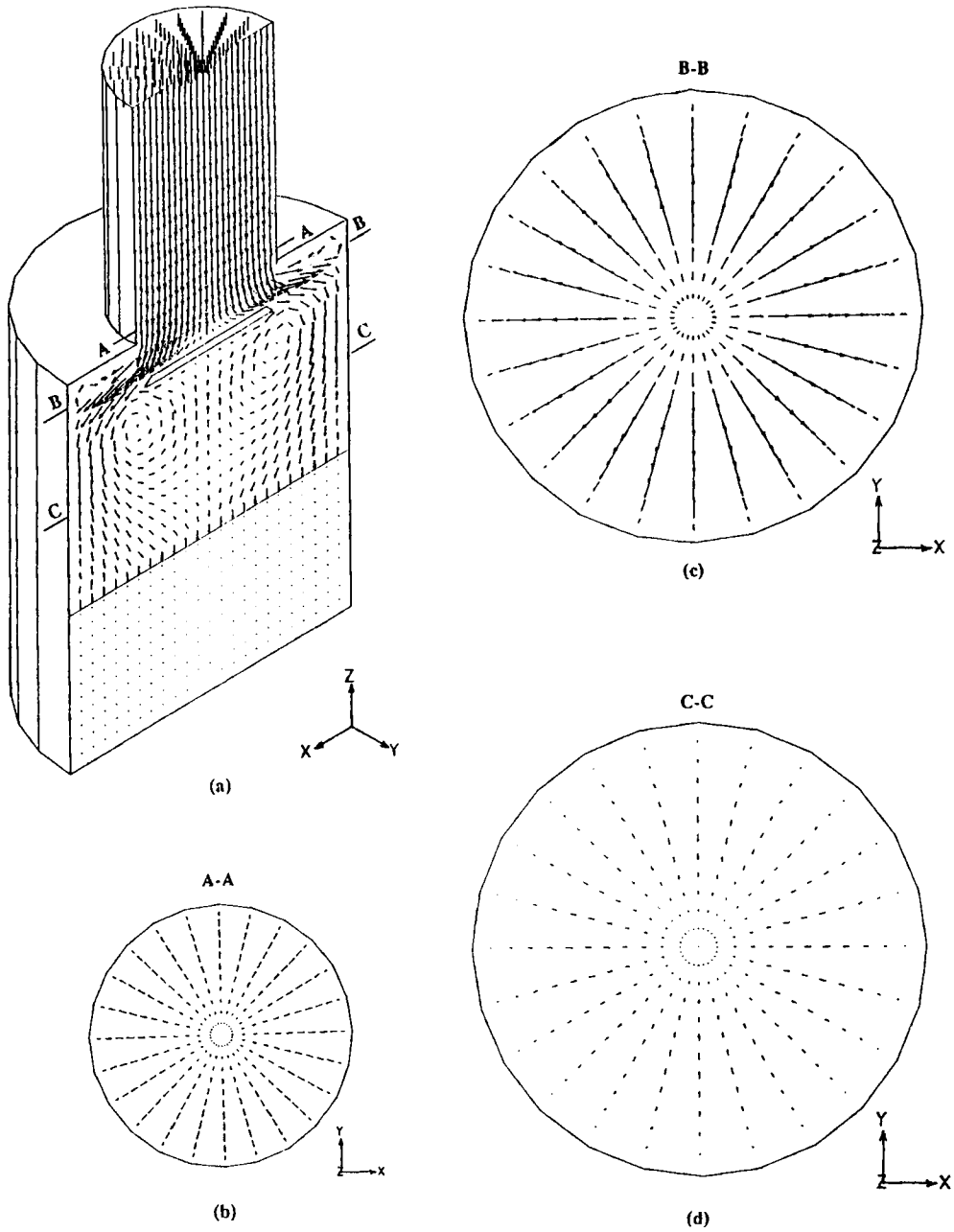

Figure 6. Velocity vector plots at an equivalent crank angle $\theta = 90°$ for the case with a central intake port

periphery is found to be non-uniform. The computed flow structure is graphically similar to the experimental pictures[31] and recent calculations[32] using a finite element method. The flow in the diameter planes, which is entirely radial, is revealed in Figures 6(b)–6(d). It can be seen from the current result that the full-geometry calculation gives rise to complete axisymmetry (as is the geometry itself). Previous axisymmetrical solutions for this type of model engine[4–6] are thus

motivated. It should be noted, however, that the assumption of uniform flow into the combustion chamber through the valve curtain area for the inlet boundary condition in the numerical simulations of Wakisaka *et al.*[7] cannot be confirmed in the present calculations.

5.3. A chamber with an off-centre intake and an off-centre exhaust port

We have examined the flow structure produced by an intake port aligned with the centre line of the chamber. Most configurations of real engines, however, are not axisymmetrical. A case for

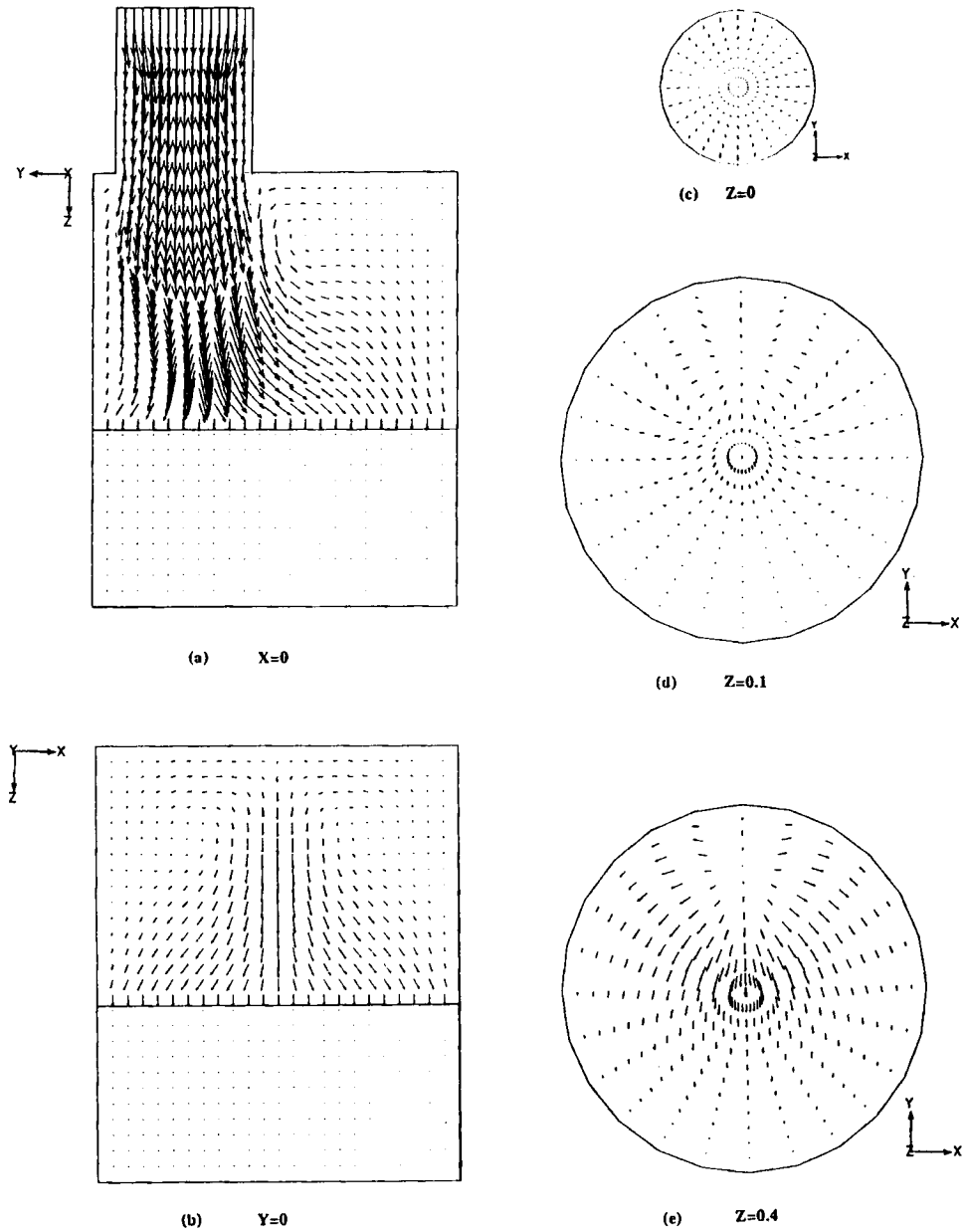

Figure 7. Velocity vector plots at an equivalent crank angle $\theta = 90°$ for the case with an off-centre intake port

which a combustion chamber is equipped with an off-centre intake and an off-centre exhaust port is computed. The overlapping-grid system used for this case is illustrated in Figure 1(a). The intake and the exhaust stubs are aligned with the mid-plane of the cylinder. There are three grid levels in each component of the grid system for the MG process. The finest grids are $13 \times 26 \times 29$ for the cylinder chamber; $9 \times 26 \times 17$ for both the intake and the exhaust ports. During the intake/exhaust stroke process the exhaust/intake port is closed. Figures 7–9 depict results of

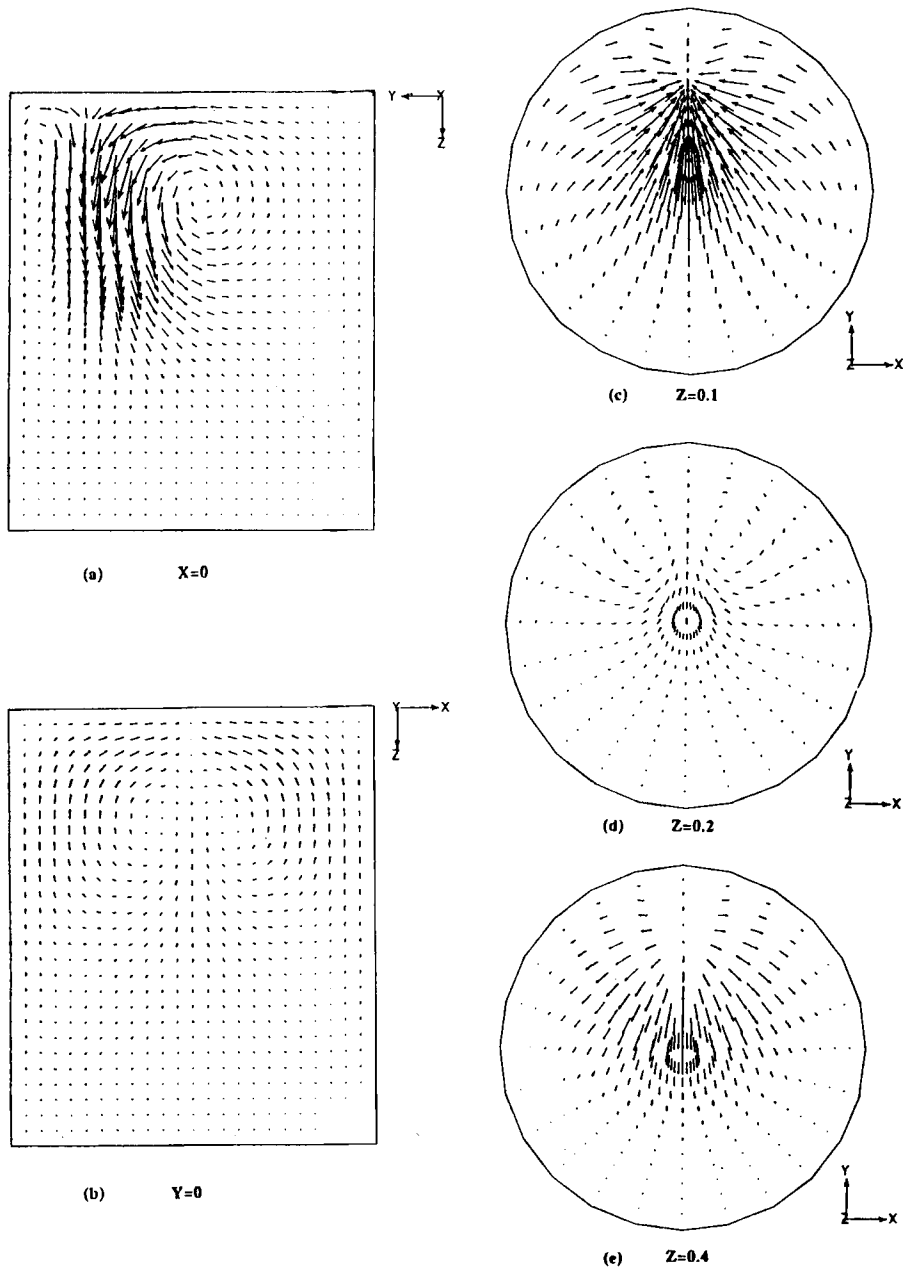

Figure 8. Velocity vector plots at an equivalent crank angle $\theta = 180°$ for the case with an off-centre intake port

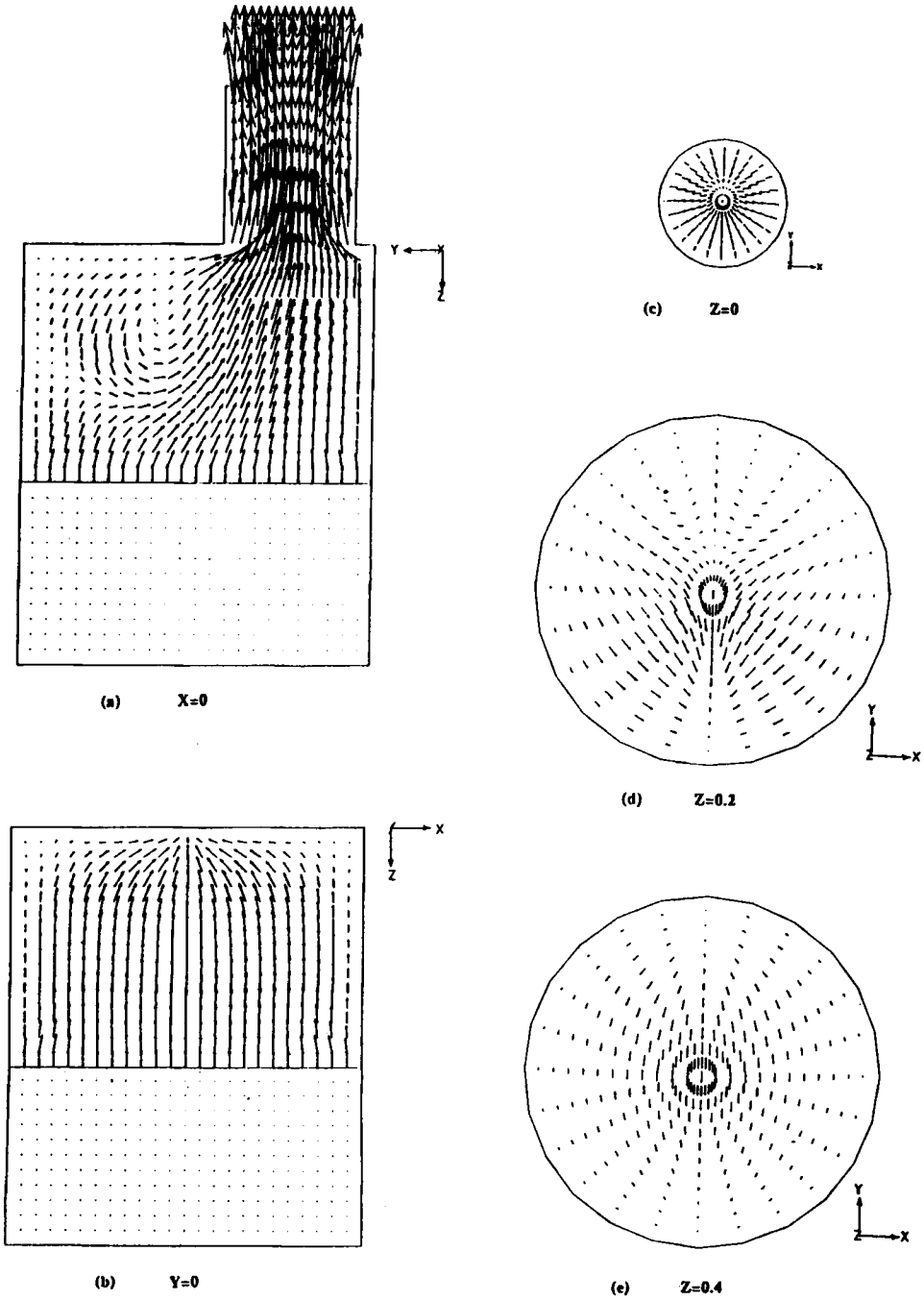

Figure 9. Velocity vector plots at an equivalent crank angle $\theta = 270°$ for the case with an off-centre exhaust port

a simulation of the flow during the intake and the exhaust stroke process, shown at different equivalent crank angles of $\theta = 90°$, 180° and 270°, respectively.

During the first half of the intake stroke (Figure 7), a primary vortex is formed near the head of the chamber on the y–z plane. The incoming jet forms two counter-rotating toroidal vortices located at the two sides of the cylinder axis on the x–z plane. The most important difference between the two flow fields induced by an off-centre intake port and a central intake port is that a swirling flow about the cylinder axis in the transverse plane, as illustrated in Figure 7(e), is created due to the off-centre position of the intake port, compared to the radial flow as shown in Figure 6(d).

Throughout induction, i.e. up to the crank angle of $\theta = 180°$, the primary vortex in the y–z plane expands in size and is confined to the upper half of the cylinder volume. In the x–z plane the centres of two counter-rotating toroidal vortices move closer to the cylinder axis and the flow between the wall and the cylinder axis in the upper half of the cylinder volume becomes stronger. Comparison of Figure 8(c) with 8(e) indicates that the plane-symmetrical swirling flows near the head and in the middle of the chamber are in the opposite directions. It is interesting to note that the flow in the transverse plane at $z = 0{\cdot}2$ is more complex as illustrated in Figure 8(d), showing two small counter-rotating vortices near the intake port.

During the exhaust stroke process, the exhaust port is assumed to be fully opened. When the piston moves away from BDC, most of the flow changes direction towards the head of the chamber (see Figure 9). This flow pattern is qualitatively similar to the experimental observations of Morse *et al.*[33] It should also be noted that the primary vortex in the y–z plane does not disappear during the exhaust stroke process at the crank angle of $\theta = 270°$. The two small vortices near the intake port in the transverse plane still remain though they become weaker [Figure 9(d)].

5.4. A chamber with multiple ports

To further confirm the capability of our technique, the flow field in a combustion chamber with multiple intake and exhaust ports is calculated. Figure 10 illustrates an example for a chamber with two intake and two exhaust ports. The computed result plotted in terms of the velocity vectors at the full induction phase, is presented in Figure 11. A comparison with the flow field

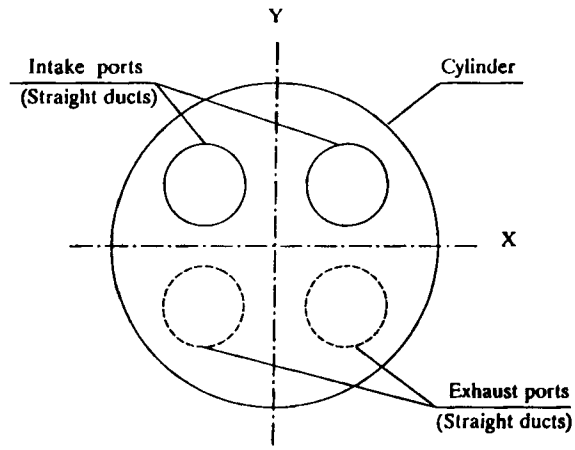

Figure 10. Illustration of a chamber with two intake or exhaust ports

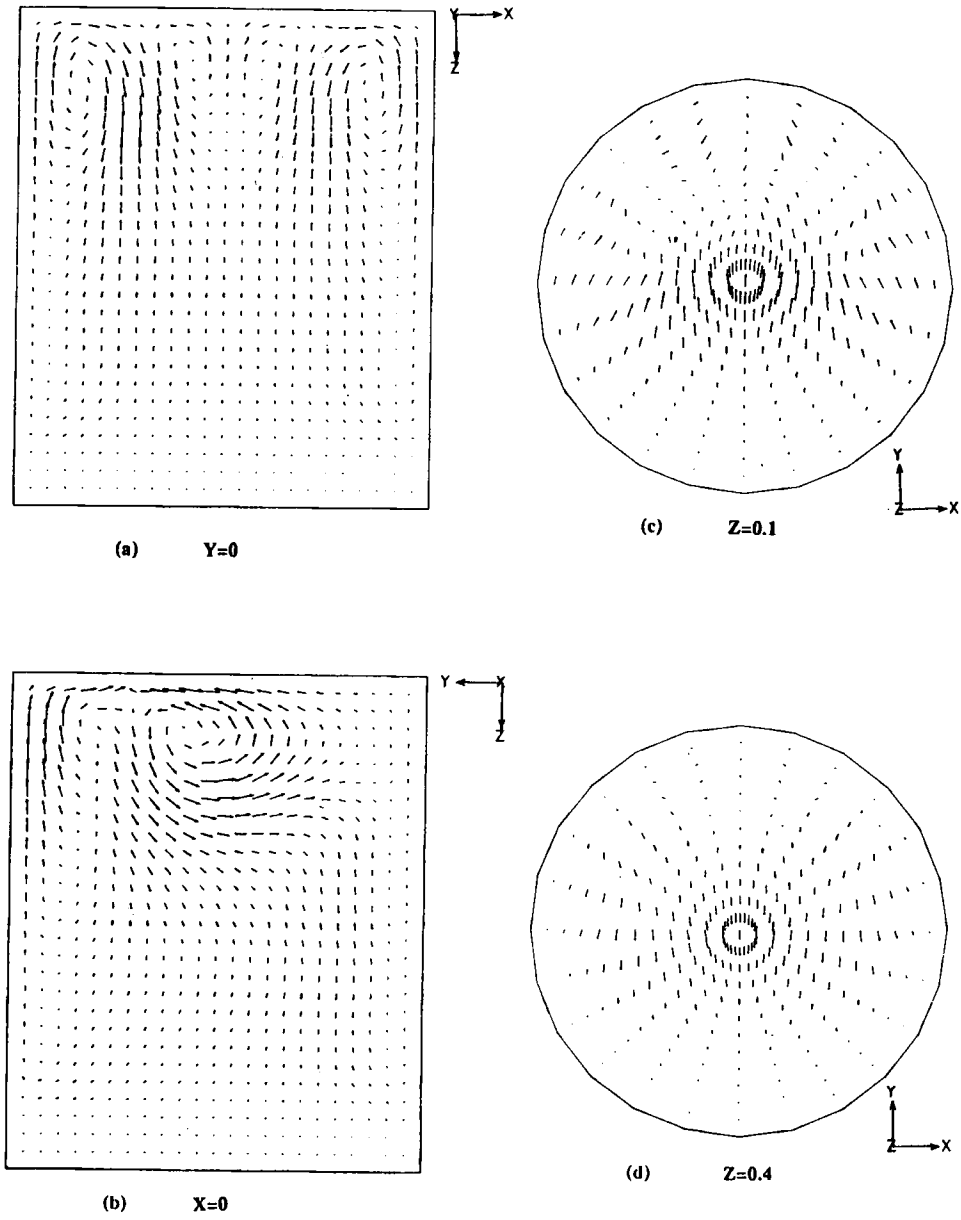

Figure 11. Velocity vector plots at an equivalent crank angle $\theta = 180°$ for the case with two intake ports

induced by one intake port as illustrated in Figure 9, reveals that the flow structure within the chamber with multiple intake ports becomes more complex.

5.5. A chamber with a curved-duct intake and a curved-duct exhaust port

A more practical configuration is a chamber fitted with an off-centre curved-duct intake and an off-centre curved-duct exhaust port. In order to increase the effect of swirl within the combustion

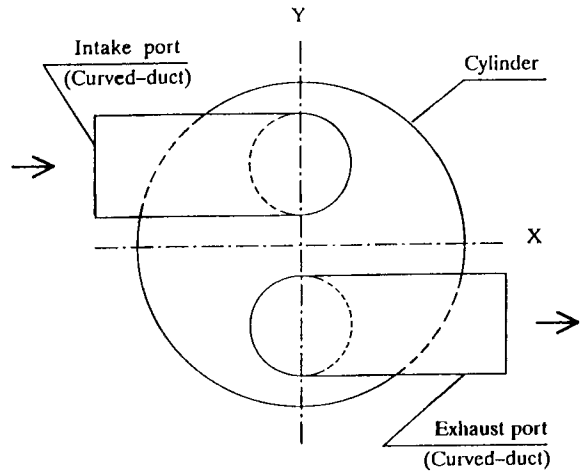

Figure 12. Illustration of an arrangement between the curved-duct ports and the cylinder chamber

chamber, an arrangement between the curved-duct ports and the combustion chamber is made similarly to that in the experimental investigation of Hirotomi *et al.*[33] as illustrated in Figure 12. Swirl is used to speed up the combustion process and to promote more rapid mixing between the induced air charge and the injected fuel. In this way, the swirl is a very important characteristic in the design process for the IC engines. With this type of induction port and arrangement, swirl within the combustion chamber can be created by bringing the flow into the cylinder with an initial angular momentum. The overlapping-grid system is illustrated in Figure 1(a), where the only difference from the present case is due to the different location of the curved-duct ports with respect to the cylinder axis. Through this case, one may recognize that the effect of geometrical factors on the flow structure in the IC engine may be examined more economically by the present numerical means than the experimental effort.

The grids used for this case are composed of three-level grids for each component in which the finest grids are $13 \times 26 \times 29$ for the chamber and $9 \times 26 \times 29$ for both the intake and the exhaust ports. Figures 13–15 depict instantaneous velocity vectors at different equivalent crank angles of $\theta = 90°$, 180° and 270°, respectively.

At the crank angle of $\theta = 90°$ (see Figure 14), the primary vortices near the head of the chamber are less evident than those revealed in Figure 7. This is because the axial flow induced by the curved-duct port into the cylinder is weaker than that induced by the straight-duct port. It is interesting to note that a tangential flow with respect to the cylinder axis from the outlet of the curved-duct intake port, as shown in Figure 13(c), is created so that a strong swirling flow near the head of the cylinder is formed as revealed in Figure 13(d). A complex flow showing a small vortex near the inlet of the cylinder is also found. Figure 13(e) depicts that a nearly plane-symmetrical swirling flow close to the piston is produced by the interaction of the intake jet flow with the piston face.

Until the full induction, the large-scale rotating flow patterns within the cylinder volume are clearly evident, as exhibited in Figures 14(a) and 14(b). Several small vortices revealing a complex flow in the diameter plane are illustrated in Figures 14(c)–14(e). The scale factor in Figures 14(d) and 14(e) is four times larger than in Figures 14(a)–14(c). The pair vortex flow pattern, shown in

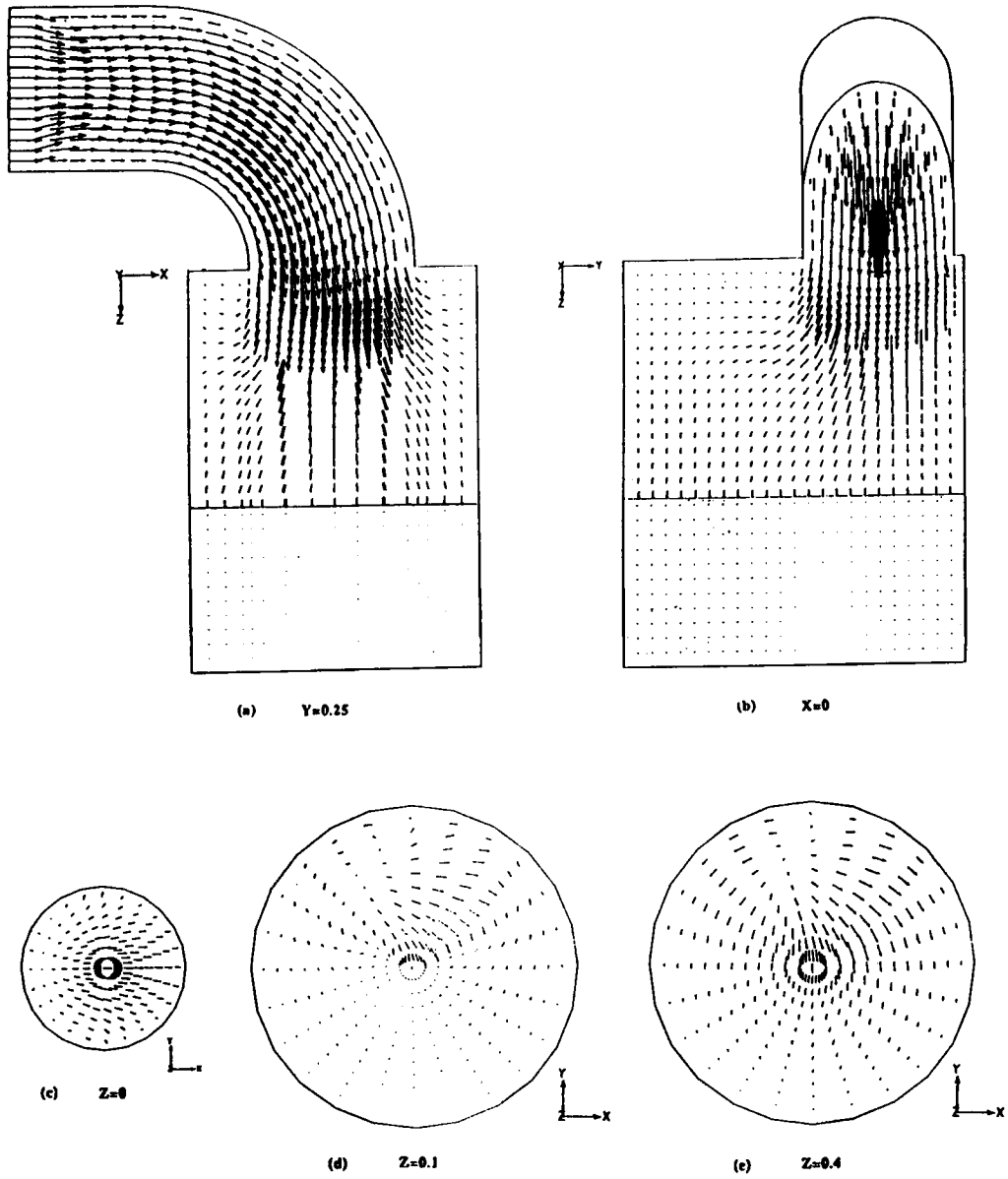

Figure 13. Velocity vector plots at an equivalent crank angle $\theta = 90°$ for the case with a curved-duct intake port

Figure 14(d), strongly resembles the one observed experimentally.[33] It is interesting to point out that a completely different form of the swirling flows induced by the curved-duct intake port has been created when comparing with a plane-symmetrical swirl flow induced by a straight duct. It should also be noted that the flow structures during the exhaust stroke process produced by the curved-duct and the straight-duct exhaust port are very similar, as seen in Figure 15 and Figure 9, respectively.

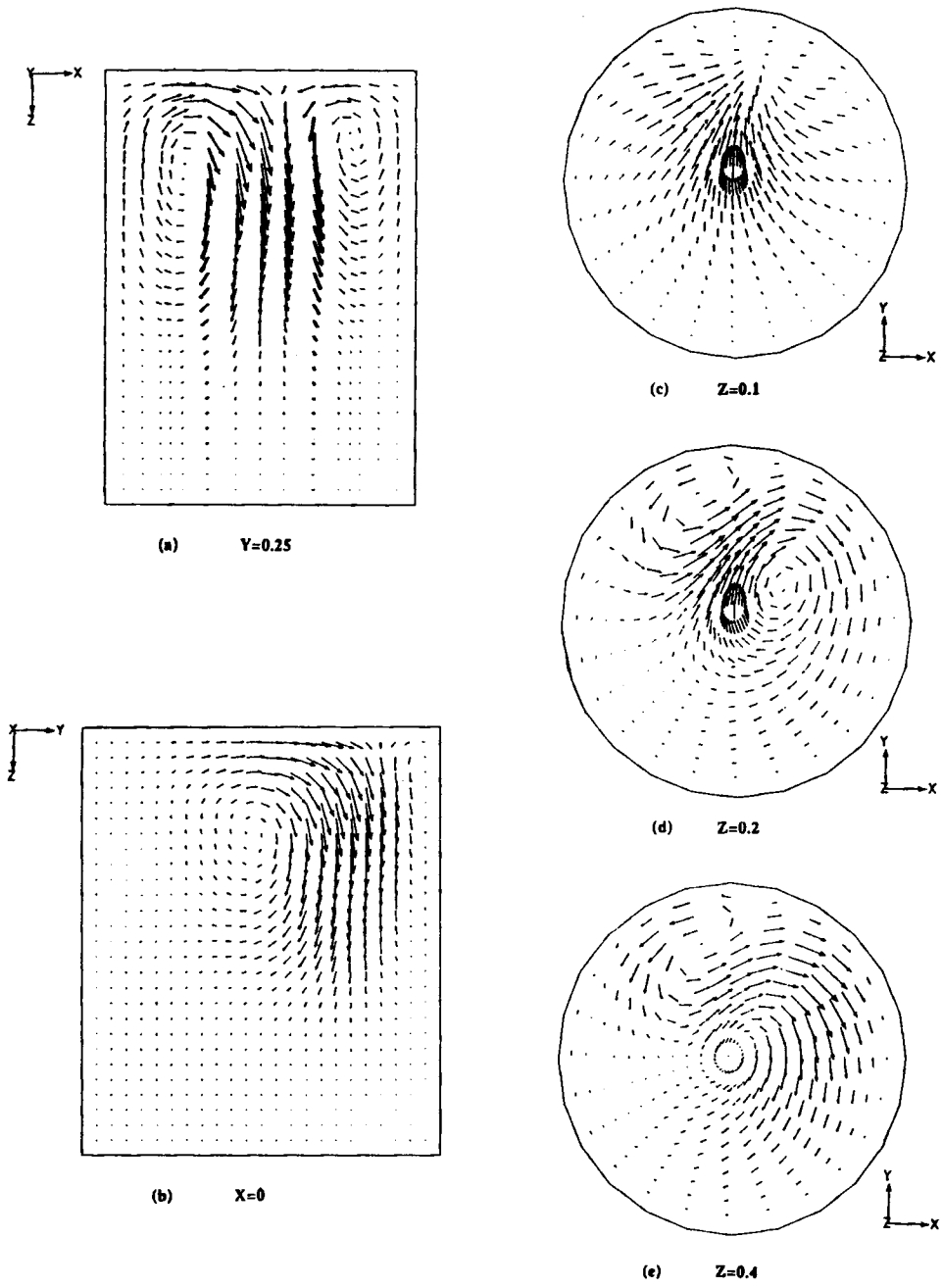

Figure 14. Velocity vector plots at an equivalent crank angle $\theta = 180°$ for the case with a curved-duct intake port

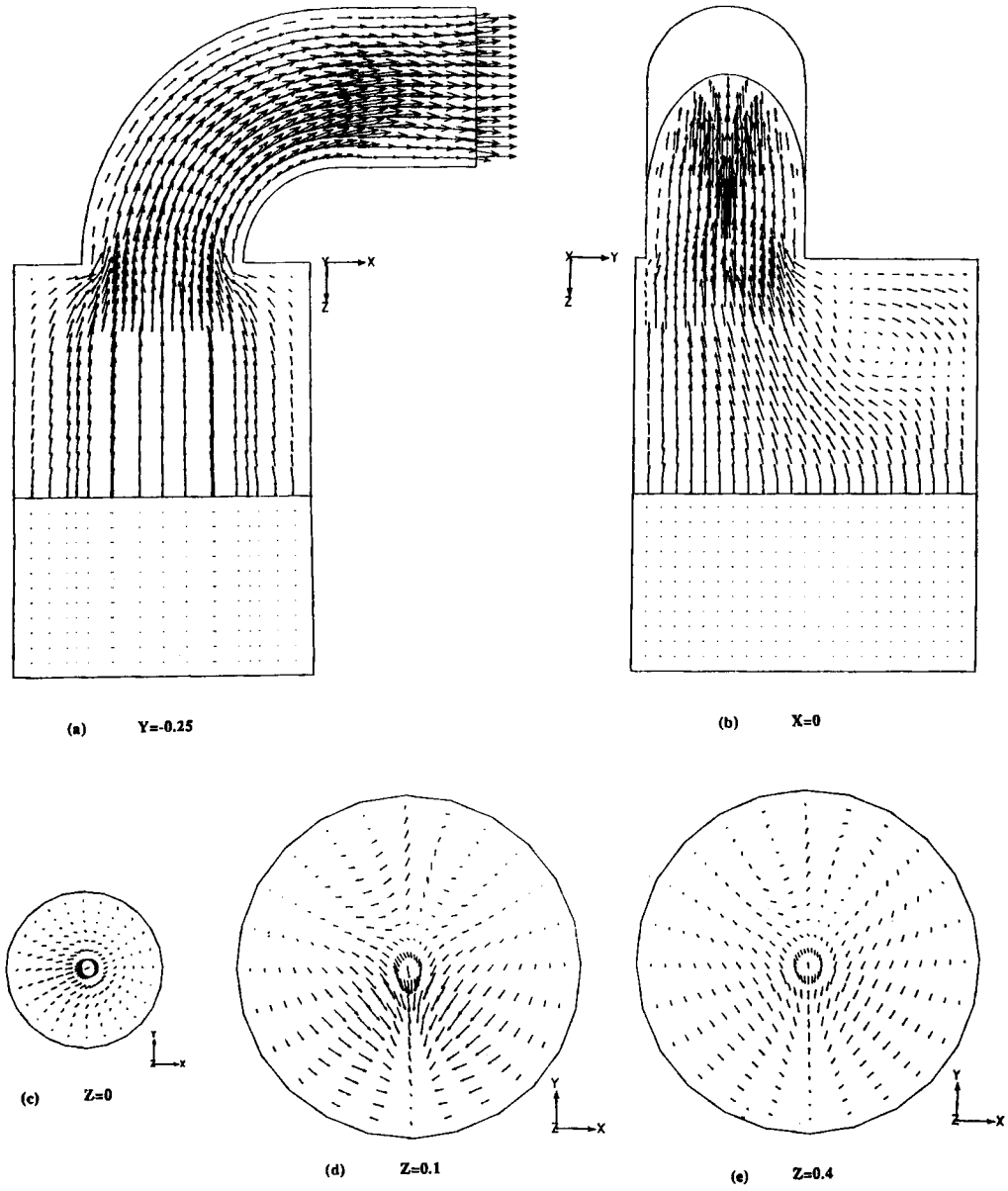

Figure 15. Velocity vector plots at an equivalent crank angle $\theta = 270°$ for the case with a curved-duct exhaust port

6. CONCLUDING REMARKS

The flow field in three-dimensional configurations of IC engines, where both the intake/exhaust port systems and the combustion chamber are simultaneously considered, has been investigated. The use of a new methodology combining the overlapping-grid technique with the multigrid method and the use of a time-independent grid system for the moving boundary in the engine problem are emphasized. The current overlapping-grid technique has enhanced flexibility and

capability in dealing with three-dimensional multicomponent time-dependent configurations. The multigrid method is incorporated into the overlapping-grid technique to allow the efficient solution of the system of PDE describing the flow. The main advantage of our overlapping-grid system is that it allows the treatment of complex engine problems without the need for grid regeneration. The MG scheme is mandatory for the overlapping-grid system to compensate for the additional reduction of computational speed due to the information exchange among the different grids. The numerical results demonstrate that the current scheme is easier and more efficient in handling the complex problem with multicomponent geometries than with the conventional single-grid scheme. The engine flow patterns from the full geometry calculation with the present method are essentially identical to those found experimentally. Currently we incorporate a $(k$–$\varepsilon)$ turbulence model into the scheme to study more realistic turbulent flow phenomena in the model IC engine. In addition, a local mesh refinement scheme is introduced at the regions where locally higher resolution is needed, such as at an area around a moving valve.

ACKNOWLEDGEMENT

This work is financially supported by the Swedish National Board for Technical Development (STU grant no. 8902268).

REFERENCES

1. A. D. Gosman, 'Computer modeling of flow and heat transfer in engines, progress and prospects', *JSME, Int. Symp. on Diagnostics and Modeling of Combustion in Reciprocating Engines*, Tokyo, 1985, pp. 15–26.
2. S. V. Patankar and D. B. Spalding, 'A calculation procedure for heat, mass and momentum transfer in 3-D parabolic flows', *Int. J. Heat Mass Transfer*, **15**, 1781–1806 (1972).
3. A. D. Gosman, R. J. R. Johns and A. P. Watkins, 'Development of prediction methods for in-cylinder processes in reciprocating engines', in J. N. Mattavi and C. A. Amann (eds), *Combustion Modeling in Reciprocating Engines*, Plenum Press, New York, 1980.
4. L.-F. Martins and A. F. Ghoniem, 'Vortex simulation of the intake flow in a planar piston-chamber device', *Int. j. numer. methods fluids*, **12**, 237–260 (1991).
5. J. I. Ramos, J. A. C. Humphrey and W. A. Sirignano, 'Numerical prediction of axisymmetric, laminar and turbulent flows in motored, reciprocating internal combustion engines', *SAE Transactions*, **88**, 1217–1242 (1979).
6. F. Grasso and F. V. Brocco, 'Computed and measured turbulence in axisymmetric reciprocating engines', *AIAA J.*, **21**, 601–607 (1983).
7. T. Wakisaka, Y. Shimamoto and Y. Isshiki, 'Three-dimensional numerical analysis of in-cylinder flows in reciprocating engines', *SAE paper 860464* (1986).
8. A. D. Gosman, Y. T. Tsui and A. P. Watkins, 'Calculation of unsteady three-dimensional flows in a model motored reciprocating engine and comparison with experiment', *Proc. 5th Int. Symp. on Turbulent Shear Flows*, Cornell University, New York, 1985.
9. M. Errera, 'Numerical prediction of fluid motion in the induction system and the cylinder in reciprocating engines', *SAE paper 870594* (1987).
10. B. Ahmadi-Befrui, A. D. Gosman, R. I. Issa and A. P. Watkins, 'EPISO—An implicit non-iterative solution procedure for the calculation of flows in reciprocating engine chambers', *Comp. Methods Appl. Mech. Eng.*, **79**, 249–279 (1990).
11. M. Reggio, J.-Y. Trepanier and R. Camarero, 'A composite grid approach for the Euler equation', *Int. j. numer. methods fluids*, **10**, 161–178 (1990).
12. M. T. Arthur, T. A. Blaylock and Anderson, 'Cell-vertex, multigrid Euler scheme for use with multiblock grids', *AIAA J.*, **29**, 507–514 (1991).
13. E. H. Atta and J. Vadyak, 'A grid overlapping scheme for flowfield computations about multicomponent configurations', *AIAA J.*, **21**, 1271–1277 (1983).
14. C.-Y. Gu and L. Fuchs, 'A non-isotropic interpolation scheme applied to zonal-grid calculation of transonic flows', in C. Taylor, W. G. Habashi and M. M. Hafez (eds), *Numerical Methods in Laminar and Turbulent Flows—V*, Pineridge Press, 1987, pp. 975–989.
15. L. Fuchs, 'Calculation of flow fields using overlapping grids', in P. Wesseling (ed.), *Notes on Numerical Fluid Mechanics*, Vol. **29**, pp. 138–147 (1990).
16. G. Chesshire and W. D. Henshaw, 'Composite overlapping meshes for the solution of partial differential equations', *J. Comput. Phys.*, **90**, 1–64 (1990).
17. A. Brandt and N. Dinar, 'Multigrid solution to elliptic flow problems', in S. V. Parter (ed.), *Numerical Methods in PDE*, Academic Press, New York, 1977, pp. 53–147.

18. L. Fuchs and H. S. Zhao, 'Solution of three-dimensional viscous incompressible flows by a multi-grid method', *Int. j. numer. methods fluids*, **4**, 539–555 (1984).
19. L. Fuchs, 'Numerical flow simulation using zonal grids', *AIAA paper* 85–1576, 1985.
20. J. Y. Tu and L. Fuchs, 'Numerical solution of time-dependent PDEs on 3-D overlapping grids', in A. S. Arcilla, J. Häuser, P. R. Eiseman, J. F. Thompson (eds), *Numer. Grid Generation in Comp. Fluid Dynamics and Related Fields*, Elsevier, Amsterdam, 1991, pp. 665–673.
21. C. M. Hung and W. Kordulla, 'A time-split finite-volume algorithm for three-dimensional flowfield simulation', *AIAA J.*, **22**, 1564–1572 (1984).
22. R. C. Swanson and R. Radespiel, 'Cell centered and cell vertex multigrid schemes for the Navier–Stokes equations', *AIAA J.*, **29**, 697–703 (1991).
23. W. Kordulla and M. Vinokur, 'Efficient computation of volume in flow prediction', *AIAA J.*, **21**, 917–918 (1983).
24. A. Jameson, 'Numerical solution of the Euler equation for compressible inviscid fluids', in F. Angrand, A. Dervieux, J. A. Desideri and R. Glowinski (eds), *Numerical Methods for the Euler Equations of Fluid Dynamics*, SIAM, Philadelphia, 1985, pp. 199–245.
25. R. C. Swanson and E. Turkel, 'Artificial dissipation and central difference schemes for the Euler and Navier–Stokes equations', *AIAA paper 87–1107*, 1987.
26. A. Karlsson and L. Fuchs, 'Fast and accurate solution of time dependent incompressible flow', in C. Taylor, J. A. Johnson, W. R. Smith (eds), *Numerical Methods in Laminar and Turbulent Flows*, Pineridge Press, 1983, pp. 606–616.
27. A. Jameson and S. Yonn, 'Multigrid solution of the Euler equation using implicit schemes', *AIAA J.*, **24**, 1737–1743 (1986).
28. W. Hackbusch, *Multi-Grid Methods and Applications*, Springer, Berlin, 1985.
29. M. Reggio and R. Camarero, 'A calculation scheme for three-dimensional viscous incompressible flows', *ASME J. Fluids Eng.*, **109**, 345–352 (1987).
30. M. Enayet, M. Gibson, A. Taylor and M. Yianneskis, 'Laser-doppler measurements of laminar and turbulent flow in a pipe bend', *Int. J. Heat Fluid Flow*, **3**, 213–219 (1982).
31. A. Ekchian and D. P. Hoult, 'Flow visualization study of the intake process of an internal combustion engine', *SAE paper 790095, SAE Trans.* **88**, 383–400 (1979).
32. M. Buffat, 'Simulation of two- and three-dimensional internal subsonic flows using a finite element method', *Int. j. numer. methods fluids*, **12**, 683–704 (1991).
33. A. P. Morse, J. H. Whitelaw and M. Yianneskis, 'Turbulent flow measurements by laser-doppler anemometry in motored piston-cylinder assemblies', *ASME J. Fluids Eng.*, **101**, 208–216 (1979).
34. T. Hirotomi, I. Nagayama, S. Kobayashi and Yamamasu, 'Study of induction swirl in a spark ignition engine', *SAE paper 810496, SAE Trans.* **90**, 1851–1867 (1981).